J Seismol
DOI 10.1007/s10950-017-9651-7

ORIGINAL ARTICLE

Source parameters of the 27th of June 2015 Gulf of Aqaba earthquake

Sattam Almadani

Received: 22 August 2016 / Accepted: 28 February 2017

Abstract On the 27 June 2015, at 15:34:03 UTC, a moderate-sized earthquake of M_w 5.0 occurred in the Gulf of Aqaba. Using teleseismic P waves, the focal mechanism of the mainshock was investigated by two techniques. The first technique used the polarities of the first P wave onsets, and the second technique was based on the normalized waveform modeling technique. The results showed that the extension stress has a NE orientation with a shallow southward plunge while the compression stress has a NW trend with a nearly shallow westward plunge, obtaining a strike-slip mechanism. This result agrees well with the typical consequence of crustal deformation resulting from the ongoing extensional to shear stress regime in the Gulf of Aqaba (NE-SW extension and NW-SE compression). The grid search method over a range of focal depths indicates an optimum solution at 15 ± 1 km. To identify the causative fault plane, the aftershock hypocenters were relocated using the local waveform data and the double-difference technique. Considering the fault trends, the spatial distribution of relocated aftershocks demarcated a NS-oriented causative fault, in consistence with one of the nodal planes of the focal mechanism solution, emphasizing the dominant stress regime in the region. Following the Brune model, the estimates of source parameters exhibited fault lengths of $0.29 \le L \le 2.48$ km, moment magnitudes of $3.0 \le M_w \le 5.0$, and stress drops of $0.14 \le \Delta\sigma < 1.14$ MPa, indicating a source scaling similar to the tectonic earthquakes related to plate boundaries.

Keywords 2015 Aqaba earthquake · Grid search technique · Focal mechanism · P wave polarity · Waveform modeling

1 Introduction

The Gulf of Aqaba, as a part of the Dead Sea transform fault zone, has a long history of major tectonic activity (Ben-Avraham et al. 1979; Alamri et al. 1991; Ben-Avraham et al. 2008). The Gulf of Aqaba represents the southern part of the Dead Sea transform fault that connects with the rifting region in the northern Red Sea to the south. Tectonically, the gulf is controlled by the relative motions between the African, Arabian, and Eurasian plates, as well as the anticlockwise rotation of Sinai Peninsula (Fig. 1). These relative motions might be responsible for the occurrence of seismic activities in the Gulf with dominant strike-slip to infrequent dip-slip mechanisms (Pinar and Turkelli 1997; Klinger et al. 1999; Hofstetter 2003; Hofstetter et al. 2003; Shamir et al. 2003; Abdel-Fattah et al. 1997, 2006, 2016). The coupling of extensional to shear movements is currently accommodated along the plate boundaries demarcated in the region (Fig. 1). The extensional stress regime is thought to be imparted from the opening of the Red Sea with a spreading rate of 1 cm/year at 25.5° N (Chu and Gordon 1998). Moreover, the shear deformation is

S. Almadani (✉)
Department of Geology and Geophysics, College of Science, King Saud University, Riyadh 11451, Saudi Arabia
e-mail: salmadani@KSU.EDU.SA

Published online: 12 March 2017

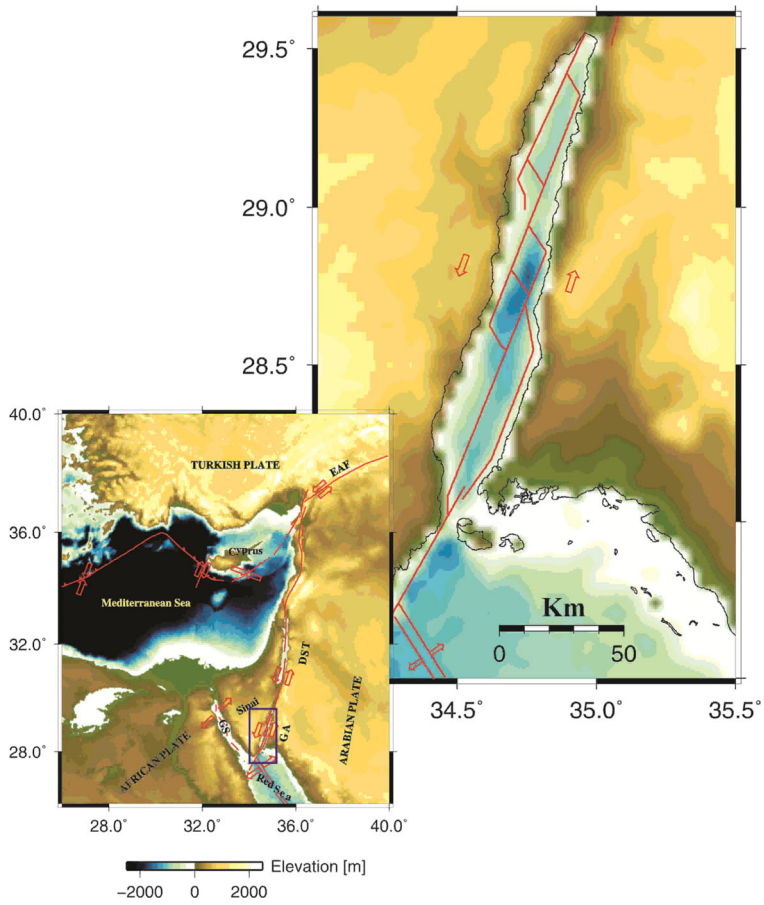

Fig. 1 Map showing three types of plate tectonic boundaries and relative plate motions in the Middle East region. The acronyms represent the following: *GA* the Gulf of Aqaba, *GS* the Gulf of Suez, *DST* Dead Sea transform, *EAF* East Anatolian Fault. The fault traces in the Gulf of Aqaba (*upper right map*) are adopted after Ben-Avraham (1985) and Darkal et al. (1990)

presumably activated by an anticlockwise rotation of the Arabian plate relative to Africa with a rate of 1 cm/year at an angle of 6° (Girdler 1966; Garson and Krs 1976).

The intense seismicity in the Gulf of Aqaba is triggered as isolated sequences (Abdel-Fattah et al. 1997). Three distinctive earthquake sequences have been reported on 1983 (M_w = 4.9, using the equation of Mohamed et al. (2012)), 1993 (M_w = 6.0), and 1995 (M_w = 7.1) for different faulting mechanisms. For instance, the 1993 earthquake exhibited pure normal faulting mechanism while the 1995 earthquake showed strike-slip focal mechanism (Pinar and Turkelli 1997; Abdel-Fattah et al. 2006). As a matter of fact, the sinistral shear slip along the strike is accommodated along the main fault trend slip of NNE orientation, while the dip slip is accommodated along the conjugate fault trend. The moment tensor summations obtained by Abdel-Fattah et al. (2016) showed average source mechanisms of pure sinistral strike-slip solutions along Aqaba-Dead sea fault.

The determination of the source mechanism, focal depth, and moment magnitude for small- to moderate-sized earthquakes is of great importance to provide insights on the ongoing stress in the region. Using different methods based on inversion and modeling techniques, the source mechanism solutions and focal depths can be determined. The solutions mainly depend on how the one-dimensional velocity model (used for computing synthetic seismograms) is adequate to reflect the simulation of true heterogeneities for low-frequency signals. This problem is resolved by computing synthetic seismograms in the frequency band lower than 0.1 Hz, giving insensitive estimates of focal depths. The region in the vicinity of the Gulf of Aqaba is characterized by different structural settings: the Dead Sea rift valley northward, the Arabian Shield eastward, the Sinai sub-plate westward, and the Red Sea rifting southward. To overcome the complex structure in the region, Abd el-aal and Badreldin (2016) retrieved the

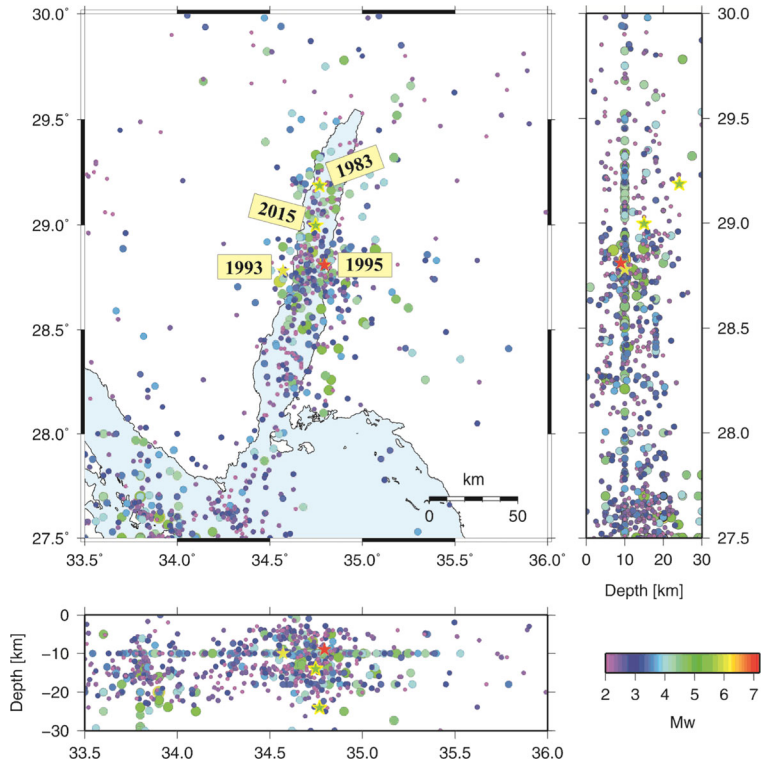

Fig. 2 The epicentral distribution map showing the earthquake data compiled from ISC in the period from 1964 to 2015. The *upper left panel* shows the spatial distribution of epicenters while the *upper right panel* and the *bottom panel* show the hypocenter distributions along the latitude and longitude, respectively. The legend classified the earthquakes with *different colors* based on the moment magnitude range. The *stars* denoted the mainshock locations of the earthquake sequences occurred in 1983, 1993, 1995, and 2015. The equation of Mohamed et al. (2012) was used to unify the moment magnitude

source mechanism of the respective earthquake using moment tensor inversion and regional waveform data recorded by seismic stations located within an azimuth beam of about 30° west. However, this narrow azimuth beam might influence the adequate estimation of the moment tensor solution.

In order to determine a precise focal depth in the present study, the focal mechanism solutions over a range of focal depths were investigated by using the waveform modeling for teleseismic P wave in a frequency band of 0.02–1 Hz. Within the distance range 30°–90°, no upper mantle triplication affects the P waves. The focal mechanism based on P wave onsets was used to constrain the focal mechanism retrieved from the waveform modeling. Considering the fault trends in the Gulf of Aqaba, the identification of the causative fault is of great importance for the seismic hazard assessments. For this purpose, the aftershock hypocenters were relocated using the double-difference technique. The source parameters were quantified using the spectral analysis technique.

2 Tectonic settings

From the geological and geophysical viewpoints, the shear deformation is accommodated along the Gulf of Aqaba-Dead Sea transform fault zone between the Arabian and African plates, advocating to be initiated less than 20 Ma BP (Freund et al. 1970; Garfunkel 1981). This tectonic process forms the complex structure in the Gulf of three successive pull-apart basins of NNE-SSW strike associated with normal to shear seismic deformations (Abdel-Fattah et al. 2016). Although the recent focal mechanism solutions and GPS studies reveal that the southern part of the Gulf undergoes extensional deformation, no direct evidence of oceanic crust has been observed.

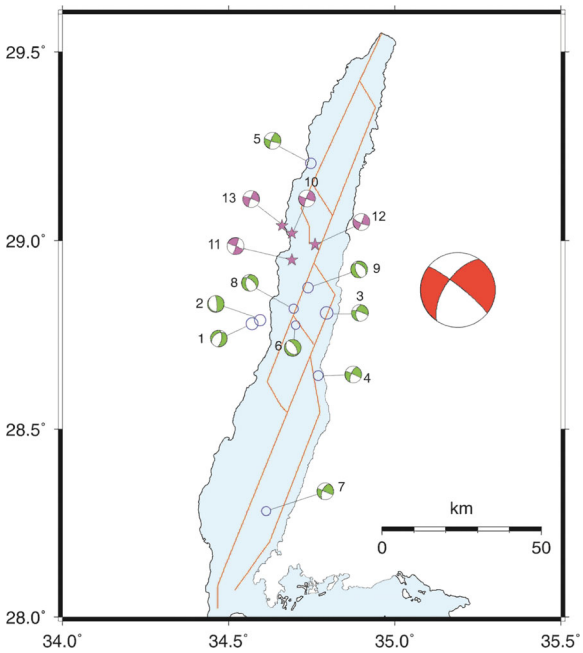

Fig. 3 The spatial distribution of locations (*open circles*) and focal mechanism solutions (*green beach balls*) for earthquakes listed from 1 to 9 in Table 1. The map also shows the average fault plane solution in the Gulf of Aqaba (*red beach ball*), as estimated from the moment tensor summation by Abdel-Fattah et al. (2016). The location (*purple stars*) and focal mechanism (*purple balls*) of the 2015 earthquake are displayed, as determined by the USGS (www.usgs.gov), GCMT (www.globalcmt.org), MED_RCMT (www.bo.ingv.it/RCMT/), and GFZ (www.gfz-potsdam.de). The *numbers* corresponded to the focal mechanism listed in Table 1

The Gulf is structurally characterized by two main faults of NNE-SSW and ESE-WNW strikes as recognized by Ben-Avraham (1985), Lyberis (1988), and Bayer et al. (1988). The faults are arranged as an echelon transverse structure, as shown in Fig. 1. The NNE-SSW fault trends control the Gulf structure with sinistral strike-slip movement that presumably initiated during the Late Miocene. The ESE-WNW faults probably originated due to the ENE-WSW extensional stress regime that began in the Late Burdigalian age (Lyberis 1988).

The source region has experienced historical earthquakes and recent seismic activities. The historical earthquakes in 600 BC, 28 BC, and 1778 are reported to have epicenters close to the center of the Red Sea (Ambraseys et al. 1994). The most recent destructive earthquake of 22 of November 1995 of M_w 7.1 is the largest earthquake that occurred along the Dead Sea transform fault and was widely felt in Egypt, Israel, Jordan, and Saudi Arabia (Abdel-Fattah et al. 2006). On the basis of GPS measurements, the average slip rate is 4.4 ± 0.3 mm/year of left-lateral deformation developed along the Gulf of Aqaba and Wadi Araba, as revealed by Mahmoud et al. (2005) and Reilinger et al. (2006). Using the moment tensor summation, the seismic slip rate showed an extensional deformation of 0.011 mm/year along ENE-WSW trend and compression of 0.007 mm/year along the NNW-SSE direction with an average focal mechanism having a strike of 204°, a dip of 62°, and a slip of −9° and similar

Table 1 The fault plane parameters for the focal mechanisms shown in Fig. 3

Author	ID	Date	Origin time	Lat. (°)	Long. (°)	Depth (km)	M_w	Strike (°)	Dip (°)	Rake (°)
NEIC	1	3/8/1993	124305.74	28.7808	34.5708	10.0	6.0	007	62	−117
HRVD	2	3/8/1993	163321.47	28.7895	34.5943	13.0	5.7	142	13	−123
NEIC	3	22/11/1995	041511.86	28.8091	34.7951	09.0	7.1	188	51	−017
HRVD	4	22/11/1995	221655.57	28.6422	34.7693	10.0	5.3	294	87	−157
HRVD	5	23/11/1995	180715.10	29.2062	34.7476	00.0	5.7	108	83	166
HRVD	6	21/2/1996	045953.67	28.8764	34.7390	22.0	5.3	132	30	−104
MED_RCMT	7	10/5/1997	230147.77	28.2817	34.6128	10.0	4.6	114	89	150
ZUR_RMT	8	8/3/2000	142225.28	28.8210	34.6950	07.0	4.9	309	57	−126
ZUR_RMT	9	6/4/2000	063733.70	28.7770	34.7020	09.0	4.4	309	41	−118
GCMT	10	27/6/2015	153402.70	29.0200	34.6900	26.0	5.6	110	88	172
MED_RCMT	11	~	153400.00	28.9500	34.69	10.0	5.5	021	85	179
GFZ	12	~	153403.00	28.9900	34.7600	17.0	5.5	022	85	−014
USGS	13	~	153403.00	29.0400	34.6600	22.0	5.6	200	84	−006

The serial numbers 10, 11, 12, and 13 corresponded to the mainshock that occurred on 27 June 2015

NEIC National Earthquake Information Center, *HRVD* Harvard University, *MED_RCMT* MedNet Regional Centroid Moment Tensors, *ZUR_RMT* Zurich Moment Tensors, *USGS* US Geological Survey, *GFZ* GeoForschungsZentrum, *GCMT* Global Centroid Moment Tensor

to the focal mechanism of the 1995 earthquake (Abdel-Fattah et al. 2016).

The seismicity and seismotectonic settings of the Gulf of Aqaba were investigated by numerous authors (El-Isa et al. 1984; Alamri et al. 1991; Shapira and Hofstetter 1993; Abdel-Fattah et al. 1997; Klinger et al. 1999; Hofstetter 2003; Salamon et al. 2003; Abdel-Fattah et al. 2006; El-Isa 2013). For earthquakes with $m_b \geq 3.0$, the moment magnitude was unified using the equation of Mohamed et al. (2012):

$$M_w = 1.16m_b - 0.9 \quad (1)$$

The seismicity in the Gulf of Aqaba from the period of 1964 to 2015, as reported by the International Seismological Center (ISC), is shown in Fig. 2. It is obvious from the figure that the hypocenter distribution shows an intensive seismicity at focal depths ranging from 5 to 20 km. The straight lines at shallow depths are probably defined by the location algorithm when the calculation provides too shallow depth. Moreover, the regional velocity model is not well calibrated in the region.

Recent focal mechanism solutions satisfied the sense of motion along the NE-SW and WNW-ESE fault trends (Abdel-Fattah et al. 1997, 2006; Pinar and Turkelli 1997, Klinger et al. 1999, Hofstetter 2003; Hofstetter et al. 2007). Figure 3 shows the available focal mechanisms that were determined by international centers (Harvard, MED_RCMT, RCMT, and ZUR_RMT) based on the assumption of double-couple point source using the moment tensor inversion technique. The parameters of the focal mechanisms are listed in Table 1. Most of the earthquakes showed normal to strike-slip faulting mechanisms. Due to the usage of different waveform dataset, it is noteworthy that the solution of MED-RCMT displayed different focal mechanisms, from all other solutions, that showed an inconsistent mechanism with the left-lateral strike-slip mechanisms along the NNE strike.

3 Data and methodology

The teleseismic P waves recorded by the broadband seismic stations were retrieved from the Data Management Center of the Incorporated Research Institutions for Seismology (IRIS). The waveforms were used to determine the

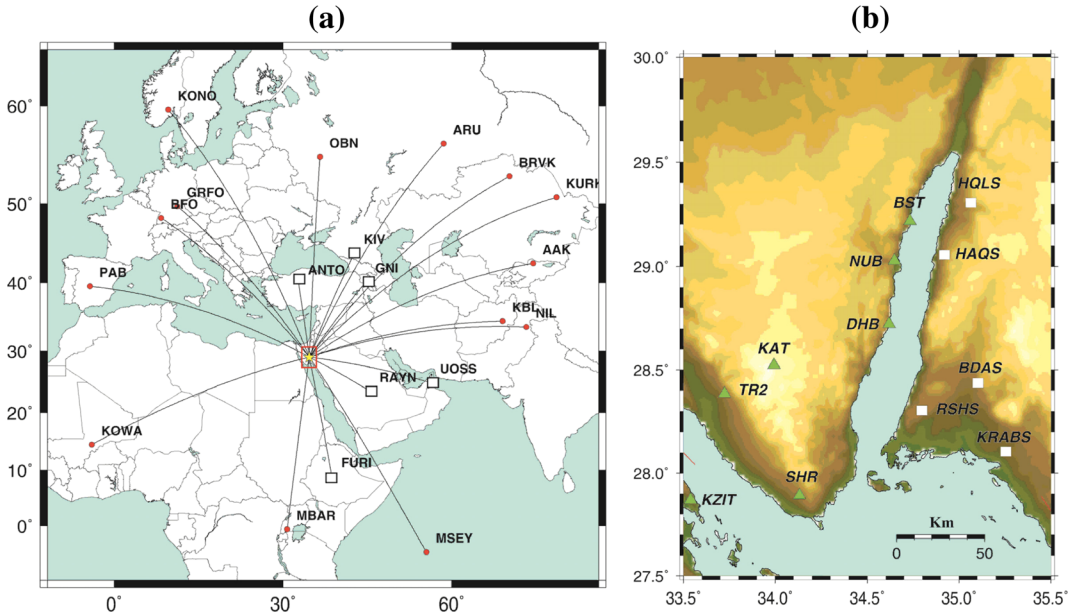

Fig. 4 Map showing the distribution of seismic stations used in the present analysis. (**a**) The location of the 2015 earthquake (*star*) and the distribution of the recorded broadband IRIS seismic stations. All stations (*solid circles* and *open squares*) are used to determine the focal mechanism using the first P wave polarities while the stations denoted by *solid circles* were used in waveform modeling. The area enclosed by *open rectangle* represented the map showed in (**b**) that displayed the distribution of local stations used to relocate hypocenters and to estimate source parameters. The *solid-triangle* stations belong to ENSN, and the *open-square* stations are for the SSN. Station codes are also written

focal mechanism, focal depth, and moment magnitude for the mainshock. The mainshock location used in the present study, as taken from the International Seismological Center (ISC), and the broadband stations are shown in Fig. 4a. The waveform data obtained from the seismic stations in Fig. 4a were used to determine the focal mechanism depending on polarities. The recordings of the seismic stations within the epicentral distance of 30°–40°, for keeping good signal-to-noise ratio, were used to determine the focal mechanism using waveform modeling. The waveform data of P wave were filtered in the frequency band of 0.02–1.0 Hz. In the solution based on P wave polarities, a total number of four stations (KONO, KURK, MSEY, and PAB) are lost as their readings are less clear. On the other hand, a total number of six stations of hypocentral distances smaller than 30° were not included in the waveform modeling.

To determine the source parameters of the mainshock and its larger aftershocks, the waveform data recorded by the Egyptian National Seismographic Network (ENSN) and the Saudi Seismographic Network (SSN) were used (Fig. 4b). The networks are operated by the National Research Institute of Astronomy and Geophysics in Egypt and the Saudi Geological Survey in Saudi Arabia, respectively.

4 Focal mechanisms

Two methods were used to retrieve the focal mechanism solution from first onset P wave polarities and waveform modeling. Firstly, the normalized waveform modeling technique incorporated with grid search technique was applied. The normalized waveform modeling for teleseismic P wave of frequency range lower than 1.0 Hz is used to show a reliable depth determination and stability in focal mechanism solutions. The green's functions were calculated using the Hudson (1969) technique and the AK135 spherical earth model of Kennett et al. (1995). Using the software developed by Herrmann and Ammon (2004), the grid search method over the strike, dip, and rake was followed to obtain the double-couple solution and the optimum focal depth. A weighted L_1 norm was summed over all stations to measure the misfit between the observed and synthetic seismograms. Secondly, the focal mechanism was determined based on P wave polarities. The theoretical travel time of the first P wave polarity was calculated using the AK135 spherical velocity model (Kennett et al. 1995) and the TauP software (Crotwell et al. 1999). The DRAWFM software program of Abdel-Fattah (personal communication), running under Linux with GUI environment, was used to project the nodal planes separating the quarters of different polarities.

The focal mechanism solutions, based on polarities and waveform modeling, showed two similar solutions of a strike-slip faulting mechanism with minor normal dip-slip component (Fig. 5). The results reflect stability in the focal mechanism solutions at different focal depths. The focal mechanism solutions, retrieved from waveform modeling, were determined at a set of focal depths through gross and fine grid searches at increments of 10° and 2°, respectively, in strike, dip, and rake. The fine grid search showed a minimum RMS value at a focal depth of 15 ± 1 km, as shown in Fig. 5. The resulted focal mechanism solution derived from waveform modeling is 354° ± 11° for strike, 61° ± 8° for dip, and −12° ± 5° for rake. Over the grid search of the double-couple solution, the standard deviation in the best-fitting solution was measured from the solutions having errors ranging from the minimum

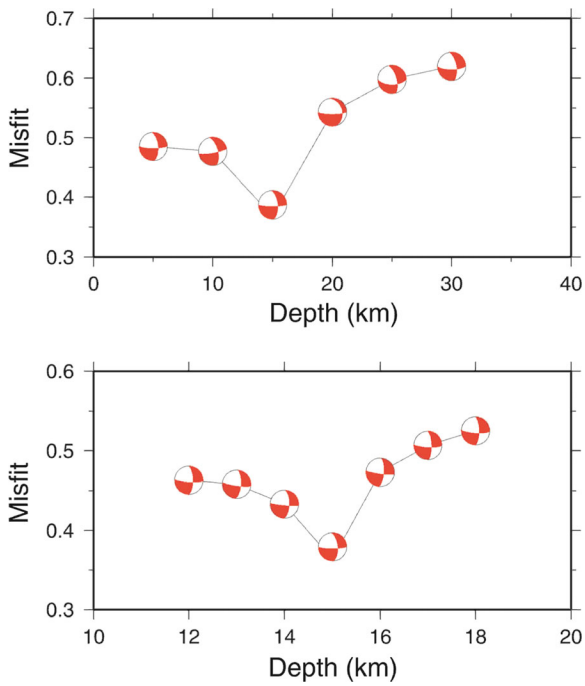

Fig. 5 Plot showing the distribution of focal mechanism solutions at different focal depths as estimated from teleseismic P wave modeling using the Hudson technique with a dislocation grid search method. The optimum solution represents the optimum focal mechanism obtained at a focal depth of 15 km and a triangle STF of 1.0s rise time

value to 10% confidence level above the minimum value. The range along the strikes, dips, and rakes is used to measure the solution uncertainty. According to the waveform modeling result, the fault plane solution is calculated by using polarities at a focal depth of 15 km. The polarity method shows a strike of 356°, a dip of 80°, and a rake of −11° (Fig. 6).

5 Double difference location

A total number of 15 aftershocks of moment magnitude larger than 2.9 were relocated using the double-difference technique (Waldhauser 2001). The differential travel time measurements of P and S waves and the velocity model of Rodgers et al. (1999) were used to relocate the events. The differential travel time was measured from the seismic stations that are shown in Fig. 4b. The distribution of relocated epicenters, with respect to the mainshock location, showed a distribution aligned in NE-SW direction, as shown in Fig. 7. The relocated hypocentral parameters are listed in Table 2.

The spatial distribution of relocated aftershocks is approximately aligned along the NS orientation in consistence with one of fault segments in the Gulf and with one of the nodal planes obtained by the fault plane solution, suggesting that the causative fault produced the 2015 Gulf of Aqaba sequence.

6 Spectral analysis

The spectrum amplitude was computed using fast Fourier transform (FFT) for the mainshock and largest aftershocks. Fourier amplitude spectrum vectorially combined the three components in the frequency domain.

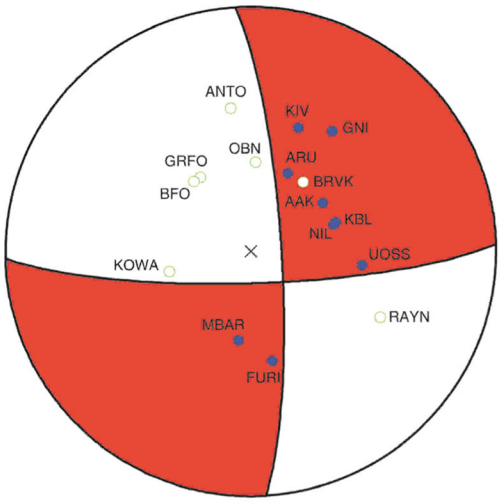

(a) Polarities

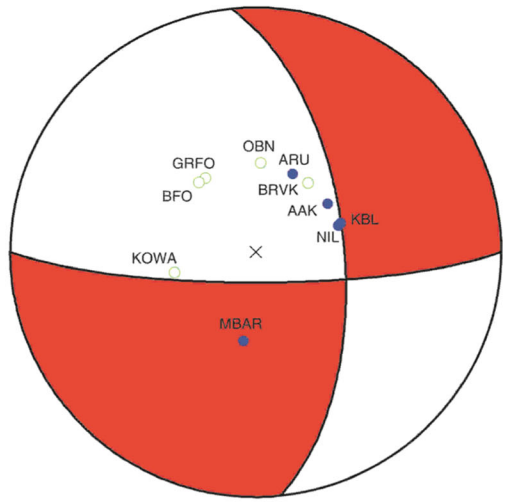

(b) Waveform inversion

	Strike	Dip	Rake
Plane NS	350	80	-2
Plane EW	80	80	-170

	Trend	Plunge
P-axis:	305	9
T-axis:	214	6

	Strike	Dip	Rake
Plane NS	354	61	-12
Plane EW	90	80	-151

	Trend	Plunge
P-axis:	316	28
T-axis:	218	13

Fig. 6 The focal mechanism solutions of the mainshock as retrieved from **a** the first arrival of P wave polarities and **b** P wave waveform inversion at a focal depth of 15 km, plotting without the stations of hypocentral distances lower than 30°. The focal mechanism retrieved from the waveform modeling displayed nearby the NS plane unmatched readings that are less clear than the other stations. The downward and upward polarities are given by *open* and *solid circles*, respectively. The *center* of the *beach ball* is denoted by the *cross symbol*. Station codes are written nearby each polarity

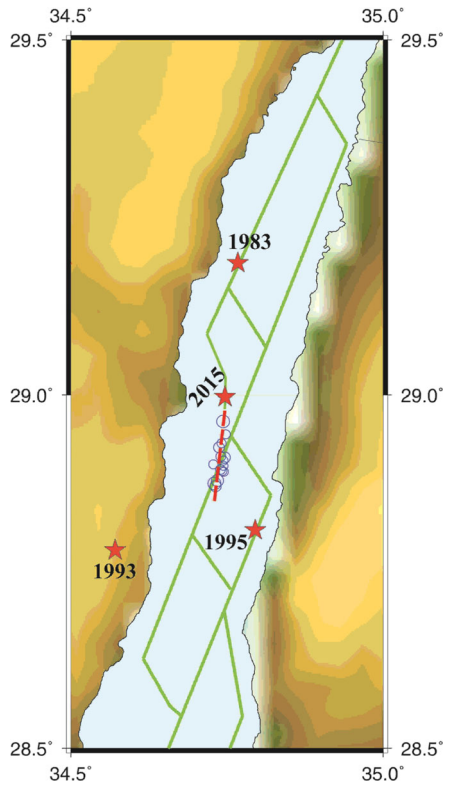

Fig. 7 The spatial distribution of the relocated aftershocks (*open circles*) with respect to the location of mainshock (*red stars*) as obtained using the double-difference algorithm. The locations (*red stars*) of 1983, 1993, and 1995 earthquakes are shown. The *dashed line* is the suggested extension of one of fault segments that is consistent with the aftershock distributions and with one of the nodal planes of focal mechanism solution obtained from the present analysis

Assuming a circular source model of the Brune model (Brune 1970), the least square technique was used to recover the model parameters, the corner frequency, and the low-frequency spectral amplitude. The spectrum amplitude was determined using time window lengths of 2–3 and 4–6 s for P and S waves, respectively.

The estimated source parameters for the mainshock and the analyzed aftershocks are listed in Table 3. Figure 8 shows the amplitude spectra of velocity waveform data. The estimated moment magnitude, fault radius, and stress drop of the mainshock are 5.0 ± 0.02, 2.48 ± 0.26 km, and 1.14 ± 0.17 MPa, respectively. The standard deviations of the source parameters were calculated by following Archuleta et al. (1982). Figure 9 shows the relationship between the seismic moment and fault radius, illustrating approximately constant stress drops. The plot is based on the dataset of mainshock and 15 aftershocks in the moment magnitude range from 3.0 to 5.0. Estimates of source parameters showed seismic moments of 3.34E+13 to 3.98E+16 Nm, fault lengths of $0.29 \leq L \leq 2.48$ km, and stress drops of 0.14 to 1.14 MPa, indicating a source scaling similar to the tectonic earthquakes related to plate boundaries.

7 Discussions and conclusions

In this study, two methods are used to retrieve the source mechanism solution of the 2015 Gulf of Aqaba earthquake. Firstly, the normalized waveform modeling that revealed strike-slip faulting mechanism of a strike of 354° ± 11°, a dip of 61° ± 8°, and a rake of −12° ± 5°; indicating an extensional stress of 13° that plunged horizontally towards N38° E and an average compressional stress of 28° that plunged towards N316° E. Secondly, the pattern of P wave polarities showed a strike-slip faulting mechanism with a strike of 350°, a dip of 80°, and a rake of −2°, indicating an extensional stress of 6° that plunged horizontally towards N34° E and a compressional stress of 9° that plunged towards N305° E.

It is noteworthy that the fault plane solution obtained from waveform modeling differs in the dip of one of the nodal planes from the pattern of the fault plane solution from the polarities (see Fig. 6). Despite the difference in the dip along the NS plane, both fault plane solutions are consistent with the regional stress pattern. The distribution of maximum and minimum compressive stresses shows mainly strike-slip stress regime with a slight extension component (horizontal NW-SE σ_1 and NE-SW σ_3). The focal mechanism solutions retrieved in the present analysis implied that the respective earthquake was the typical consequence of crustal deformation due to current tectonics, reflecting the NE-SW extension and NW-SE compression along the Gulf of Aqaba (Lyberis 1988; Bajous and Mikbel 1990; Abdel-Fattah et al. 1997; Lunina et al. 2005; Hussein et al. 2013; Abdel-Fattah et al. 2016). Under this stress regime, the dominant compatible focal mechanisms are strike-slip faulting types with fault planes dipping at a nearly vertical angle.

The present results incorporated with those obtained from earthquake focal mechanism analysis in previous studies indicate that the Gulf of Aqaba is influenced by the NW-SE compression and NE-SW extension (Abdel-Fattah et al. 1997; Hofstetter 2003; Abdel-Fattah et al. 2006, 2016). For instance, the 1995 earthquake exhibited source mechanism solution similar to that obtained in the present study,

Table 2 The location of the largest aftershocks using the double-difference algorithm

Date	O.T.	Lat. (°)	Long. (°)	Depth (km)	Δx (km)	Δy (km)	Δz (km)
27/6/2015	155001	28.8927	34.7428	14.72	0.38	0.54	0.64
27/6/2015	170703	28.7706	34.7314	14.27	0.35	0.48	0.69
27/6/2015	203601	28.9022	34.7279	12.16	0.66	0.71	0.83
27/6/2015	230225	28.9135	34.7398	14.43	0.34	0.52	0.68
28/6/2015	012852	28.9260	34.7373	11.92	0.38	0.61	0.77
28/6/2015	082752	28.8747	34.7296	11.64	0.31	0.47	0.68
28/6/2015	092341	28.9001	34.7443	12.00	0.42	0.66	0.79
28/6/2015	233828	28.8944	34.7393	12.94	0.37	0.74	0.91
29/6/2015	070236	28.8880	34.7345	13.77	0.63	0.82	0.94
29/6/2015	141023	28.9076	34.7445	14.05	0.44	0.72	0.83
30/6/2015	122853	28.9116	34.7464	13.14	0.58	0.78	0.89
7/7/2015	000155	28.9446	34.7477	12.89	0.85	0.97	1.15
7/7/2015	224036	28.8922	34.7452	10.04	0.67	0.88	0.96
8/7/2015	021534	28.9526	34.7435	13.06	0.73	0.92	1.00
9/7/2015	213022	28.9319	34.7413	12.50	0.68	0.79	0.86

Δx, Δy, and Δz are the errors in latitude, longitude, and depth, respectively. O.T. is the origin time

reflecting a maximum compressive stress axis of NW-SE orientation (Abdel-Fattah et al. 1997). Moreover, the 1993 earthquake that has occurred onshore of the eastern coast of the Gulf of Aqaba had a well-determined maximum compressive stress axis striking due NW-SE (Abdel-Fattah et al. 2006). The crustal deformation analysis based on moment tensor summation revealed that the present-day stress field in the Gulf is dominated by the NW-SE compression and NE-SW extension, whose azimuths are 135° and 45°, respectively (Abdel-Fattah et al. 2016), and is consistent with the results derived from the stress tensor inversion analysis by Hussein et al. (2013). The results are almost compatible with the geological

Table 3 Averaged source parameters (seismic moment Mo, fault radius r_o, stress drop $\Delta\sigma$, and moment magnitude M_w) for the mainshock and largest aftershocks of the 2015 earthquake sequence

ID	Event	Mo (Nm)	r_o (km)	$\Delta\sigma$ (MPa)	M_w
Mainshock	27/06/2015 15:34	3.98E+16	2.48	1.14	5.0
AF1	27/06/2015 15:50	4.21E+13	0.41	0.27	3.0
AF2	27/06/2015 17:07	1.64E+14	0.80	0.14	3.4
AF3	27/06/2015 20:36	6.85E+13	0.47	0.29	3.2
AF4	27/06/2015 23:02	4.36E+13	0.29	0.78	3.1
AF5	28/06/2015 01:28	7.50E+13	0.38	0.64	3.2
AF6	28/06/2015 08:27	6.37E+15	1.39	1.04	4.5
AF7	28/06/2015 09:23	3.74E+13	0.26	0.93	3.0
AF8	28/06/2015 23:38	7.71E+13	0.41	0.49	3.2
AF9	29/06/2015 07:02	7.77E+14	0.82	0.62	3.9
AF10	29/06/2015 14:10	3.34E+13	0.45	0.16	3.0
AF11	30/06/2015 12:28	1.94E+14	0.70	0.25	3.5
AF12	07/07/2015 00:01	3.83E+13	0.41	0.24	3.0
AF13	07/07/2015 22:40	4.96E+13	0.40	0.34	3.1
AF14	08/07/2015 02:15	2.96E+15	1.06	1.10	4.3
AF15	09/07/2015 21:30	4.99E+13	0.37	0.43	3.1

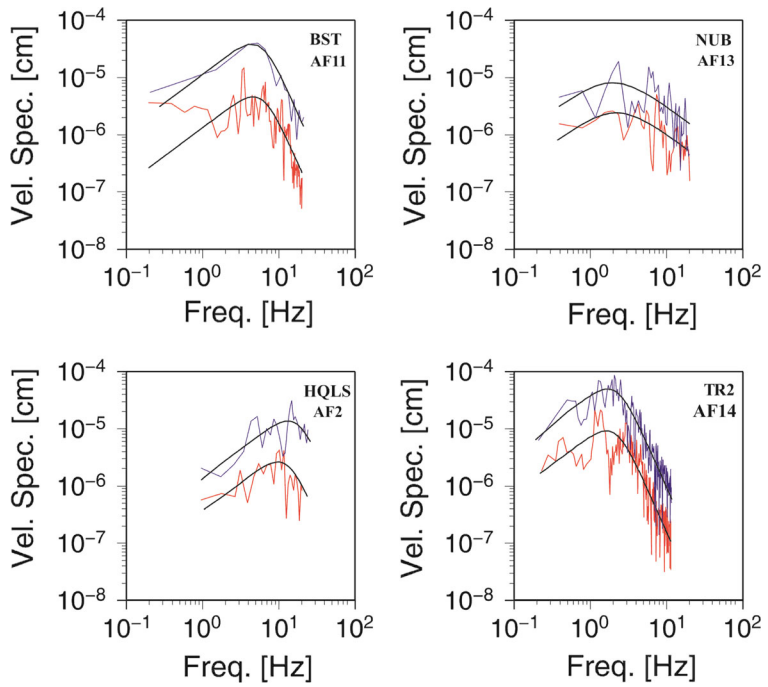

Fig. 8 Plot showing the velocity spectra and the corresponding synthetic spectra (*black lines*) for selected stations and events for P wave (*red lines*) and S-wave (*blue lines*). A grid search technique, combined with an assumption of circular source model, was applied to find the best-fit source spectra over the space parameters: long period spectral level and corner frequency assuming the asymptotic high-frequency falloff of 2. The station code and the event ID are written on the *upper right* for each *panel*. The event ID corresponded to the event serial number listed in Table 3

evidence, ERS-SAR interferometry, and the GPS observations (Klinger et al. 1999, 2000; El-Fiky 2005; Mahmoud et al. 2005).

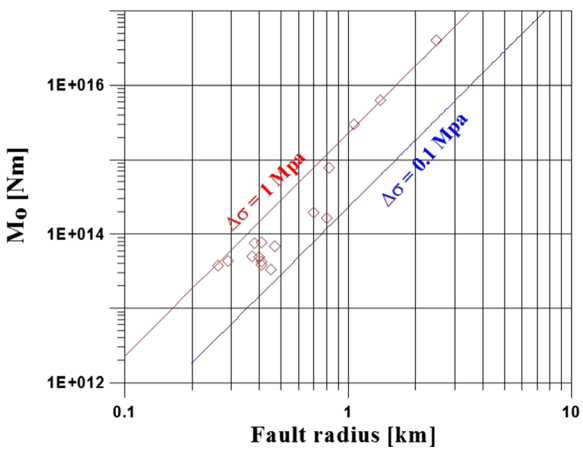

Fig. 9 Seismic moment versus fault radius of the mainshock and a total number of 15 aftershocks. *Solid lines* showed constant stress drops around 0.1 and 1 MPa. For the events of small fault radius, the stress drops are essentially below 1 MPa, while for those having larger fault radius, the stress drops are approximately closed to 1 MPa

Compiling the focal mechanism solution of the mainshock and the aftershock relocations, as obtained by the double-difference technique, the NS trending fault plane is considered as the causative fault that produced the 2015 earthquake sequence, coinciding with one of the fault segments in the Gulf. The distribution of aftershocks along the NS plane, as retrieved from the focal mechanism, suggests a reactivation of sinistral high-angle fault by the contemporary NE horizontal extensive stress, corresponding to the regional stress regime. It is noteworthy that the aftershocks are spatially distributed to the south of the mainshock epicenter.

Assuming the Brune model (Brune 1970), the estimates of source parameters exhibited fault radius of 0.3–2.42 km and the corresponding stress drops 0.14–1.14 MPa. The results reflected stress drop values similar to the tectonic earthquakes occurring along the plate boundaries, as suggested by Scholz (1990). It is noteworthy that the moment magnitude (M_w = 5.0) of the mainshock determined by spectral amplitudes for P and S waves is smaller than that published by Abd el-aal and Badreldin (2016) of 5.2, GCMT (5.6), MED_RCMT (5.5), GFZ (5.5), and USGS (5.6) using regional and

teleseismic waveform inversions. The significant difference may be due to the usage of different datasets and techniques and the uncertainties in the preliminarily determinations by the international centers.

Acknowledgements This work was supported by King Saud University, Deanship of Scientific Research, College of Science Research Centre. The author would like to thank the two anonymous reviewers for their critical reviews and comments that improved the manuscript. Generic Mapping Tools developed by Wessel and Smith (1991) was used for data mapping.

References

Abd el-aal AK, Badreldin H (2016) Seismological aspects of the 27 June 2015 Gulf of Aqaba earthquake and its sequence of aftershocks. J Seismol 20:935–952

Abdel-Fattah AK, Hussein HM, Ibrahim EM, Abu El Atta AS (1997) Fault plane solutions of the 1993 and 1995 Gulf of Aqaba earthquakes and their tectonic implications. Ann Geofis XL(6):1555–1564

Abdel-Fattah AK, Hussein HM, El-Hady S (2006) Another look at the 1993 Mw=6.1 and Mw=7.2 Gulf of Aqaba earthquakes from the analysis of teleseismic waveforms. J Acta Geophysica 54(3):260–279

Abdel-Fattah AK, Mogren S, Almadani S (2016) Seismicity constraints on stress regimes along Sinai subplate boundaries. Stud Geoph Geod 60(2):268–279

Alamri A, Schult F, Bufe C (1991) Seismicity and aeromagnetic features of the Gulf of Aqaba region. J Geophys Res 96(B12):179–185

Ambraseys NN, Melville CP, Adams RD (1994) The seismicity of Egypt, Arabia and the Red Sea: a historical review. Cambridge University Press, Cambridge

Archuleta RJ, Cranswick EC, Mueller C, Spudich P (1982) Source parameters of the 1980 Mammoth Lakes, California, earthquake sequence. J Geophys Res 87:4595–4607

Bajous M, Mikbel S (1990) Tectonic evolution of the Gulf of Aqaba-Dead Sea transform fault system. Tectonophysics 180:49–59

Bayer HJ, Hotzl H, Jado AR, Roscher B, Voggenreiter W (1988) Sedimentary and structural evolution of the north-west Arabian Red Sea Margin. Tectonophysics 153:137–151

Ben-Avraham Z (1985) Structural framework of the Gulf of Elat (Aqaba), northern Red Sea. J Geophys Res 90:703–726

Ben-Avraham Z, Almagor G, Garfunkel Z (1979) Sediment and structure of the Gulf of Elat (Aqaba)-Northern Red Sea. Sediment Geol 23:239–267

Ben-Avraham Z, Garfunkel Z, Lazar M (2008) Geology and evolution of the southern Dead Sea Fault with emphasis on subsurface structure. Annu Rev Earth Planet Sci 36:357–387

Brune JN (1970) Tectonic stress and the spectra of seismic shear waves from earthquakes. J Geophys Res 75:4997–5009

Chu D, Gordon RG (1998) Current plate motions across the Red Sea. Geophys J Int 135:313–328

Crotwell PH, Owens TJ, Ritsema J (1999) The TauP toolkit: flexible seismic travel-time and ray-path utilities. Seismol Res Lett 70:154–160

Darkal AN, Krauss M, Ruske R (1990) The Levant fault zone. An outline of its structure, evolution and regional relationship. Z Geol Wiss Berlin 18:549–562

El-Fiky G (2005) GPS-derived velocity and crustal strain field in the Suez-Sinai area, Egypt. Bull Earthq Res Inst Univ Tokyo 80:73–86

El-Isa ZH (2013) Seismicity and seismotectonics of the Gulf of Aqaba region. Arab J Geosci 6:3437–3449

El-Isa Z, Merghelani H, Bazzari M (1984) The Gulf of Aqaba earthquake swarm of 1983 January-April. Geophys J Int 78: 711–722

Freund R, Garfunkel Z, Zak I, Goldberg M, Weissbrod T (1970) The shear along the Dead Sea rift. Phil Trans R Soc Lond A: Math Phys Sci 267:105–127

Garfunkel Z (1981) Internal structure of the Dead Sea leaky transform (rift) in relation to plate kinematics. Tectonophysics 80:81–108

Garson MS, Krs M (1976) Geophysical and geological evidence of the relationship of Red Sea transverse tectonics to ancient fractures. Bull Geol Soc Am 87:169–181

Girdler RW (1966) In: The role of translational and rotational movement in the formation of the Red Sea and Gulf of Aden: Proceed. Sym. World Rift Systems, Ottawa 1965. Geol Sur Canada Paper, pp. 65E77:66–14

Herrmann RB, Ammon CJ (2004) Computer programs in seismology. Manual of the Generic Seismic Application Coding (GSAC), Version 3.30. Saint Louis University

Hofstetter A (2003) Seismic observations of the 22/11/2015 Gulf of Aqaba earthquake sequence. Tectonophysics 369(1–2): 21–36

Hofstetter R, Thio KK, Shamir G (2003) Source mechanism of the 22/11/95 Gulf of Aqaba Earthquake and its aftershock sequence. J Seismol 7:99–114

Hofstetter R, Klinger Y, Amrat A, Rivera L, Dorbath L (2007) Stress tensor and focal mechanisms along the Dead Sea fault and related structural elements based on seismological data. Tectonophysics 429:165–181

Hudson JA (1969) A quantitative evaluation of seismic signals at teleseismic distances-I radiation from point sources. Geophys J Int 18(3):233–249

Hussein HM, Abou Elenean KM, Marzouk IA, Korrat IM, Abu El-Nader IF, Ghazala H, ElGabry MN (2013) Present-day tectonic stress regime in Egypt and surrounding area based on inversion of earthquake focal mechanisms. J Afr Earth Sci 81:1–15

Kennett BLN, Engdahl ER, Buland R (1995) Constraints on seismic velocities in the Earth from traveltimes. Geophys J Int 122:108–124

Klinger Y, Rivera L, Haessler H, Maurin J (1999) Active faulting in the Gulf of Aqaba: new knowledge from the Mw 7.3 earthquake of 22 November 1995. Bull Seismol Soc Am 89:1025–1036

Klinger Y, Michel R, Avouac J-P (2000) Co-seismic deformation during the Mw 7.3 Aqaba earthquake (1995) from ERS-SAR interferometry. Geophys Res Lett 72:3651–3654

Lunina OV, Mart Y, Gladkov AS (2005) Fracturing patterns, stress fields and earthquakes in the Southern Dead Sea rift. J Geodyn 40:216–234

Lyberis N (1988) Tectonic evolution of the Gulf of Suez and the Gulf of Aqaba. Tectonophysics 153:209–220

Mahmoud S, Reilinger R, McClusky S, Vernant P, Tealeb A (2005) GPS evidence for northward motion of the Sinai block: implications for E. Mediterranean tectonics. Earth Planet Sci Lett 238:217–227

Mohamed AA, El-Hadidy M, Deif A, Abou Elenean K (2012) Seismic hazard studies in Egypt. NRIAG J Astro and Geophys 1(2):119–140

Pinar A, Turkelli N (1997) Source inversion of the 1993 and 1995 Gulf of Aqaba earthquakes. Tectonophysics 293:279–288

Reilinger RE, Mcclusky SC, Vernant P, Lawrence S, Ergintav S, Çakmak R, Nadariya M, Hahubia G, Mahmoud S, Sakr K, Arrajehi A, Paradissis D, Al-Aydrus A, Prilepin M, Guseva T, Evren E, Dmitritsa A, Filikov SV, Gomes F, Al-Ghazzi R, Karam G (2006) GPS constraints on continental deformation in the Africa-Arabia-Eurasia continental collision zone and implications for the dynamics of plate interactions. J Geophys Res 111:B5. doi:10.1029/2005JB004051

Rodgers A, Walter W, Mellors R, Alamri A, Zhang Y (1999) Lithospheric structure of the Arabian Shield and Platform from complete regional waveform modelling and surface wave group velocities. Geophys J Int 138:871–878

Salamon A, Hofstetter A, Garfunkel Z, Ron H (2003) Seismotectonics of the Sinai subplate-the eastern Mediterranean. Geophys J Int 155:149–173

Scholz CH (1990) The mechanics of earthquakes and faulting. Cambridge Univ. Press, Cambridge 439 pp

Shamir G, Baer G, Hofstetter A (2003) Three-dimensional elastic earthquake modeling based on integrated seismological and InSAR data the Mw=7.2 Nuweiba earthquake, Gulf of Elat/Aqaba, 1995 November. Geophys J Int 154:731–744

Shapira A, Hofstetter H (1993) Source parameters and scaling relationships of earthquakes in Israel. Tectonophysics 217: 217–226

Waldhauser F (2001) HypoDD—a program to compute double-difference hypocenter locations, U.S. Geological Survey, Open File Report 01–113

Wessel P, Smith W (1991) Free software helps maps and display data. EOS Trans Am Geophys Union 72:441